JCTC Journal of Chemical Theory and Computation

Article

pubs.acs.org/JCTC

A Hybrid Density Functional Theory/Molecular Mechanics Approach for Linear Response Properties in Heterogeneous Environments

Zilvinas Rinkevicius,*[,†,‡] Xin Li,[†] Jaime A. R. Sandberg,[†] Kurt V. Mikkelsen,[§] and Hans Ågren[†]

[†]Division of Theoretical Chemistry & Biology, School of Biotechnology, KTH Royal Institute of Technology, S-106 91 Stockholm, Sweden

[‡]KTH Royal Institute of Technology, Swedish e-Science Research Centre, S-100 44 Stockholm, Sweden

[§]Department of Chemistry, University of Copenhagen, Universitetsparken 5, 2100 Copenhagen, Denmark

ABSTRACT: We introduce a density functional theory/molecular mechanical approach for computation of linear response properties of molecules in heterogeneous environments, such as metal surfaces or nanoparticles embedded in solvents. The heterogeneous embedding environment, consisting from metallic and nonmetallic parts, is described by combined force fields, where conventional force fields are used for the nonmetallic part and capacitance−polarization-based force fields are used for the metallic part. The presented approach enables studies of properties and spectra of systems embedded in or placed at arbitrary shaped metallic surfaces, clusters, or nanoparticles. The capability and performance of the proposed approach is illustrated by sample calculations of optical absorption spectra of thymidine absorbed on gold surfaces in an aqueous environment, where we study how different organizations of the gold surface and how the combined, nonadditive effect of the two environments is reflected in the optical absorption spectrum.

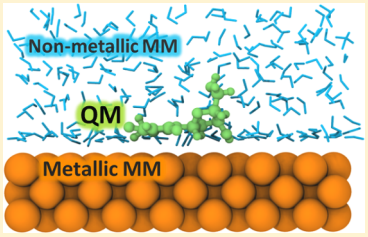

INTRODUCTION

In recent years, integrated multiscale approaches have been boosted as in silico tools with great potential for design of microscopic devices. In these approaches, the system is sampled by quantum or classical molecular dynamics simulations, generating trajectories out of which system conformations are sampled and extracted for use in the modeling of the properties or spectra, which then are averaged over the sample configurations for the final output result.[1,2] The procedure for the property calculations often involves multiscale modeling in terms of combining quantum mechanics (QM) with molecular mechanics (MM) and/or the polarizable continuum (PCM) models,[2−4] where the inherent algorithms are twinned together. Full or partial coupling in terms of intermolecular interactions (electrostatics, induction, dispersion, short-range repulsion) are taken into account between the QM and MM parts of the system, where each interaction "acts both ways". The MM part is typically described by nonpolarizable or polarizable force fields with parameters (point charges, distributed polarizabilities) determined empirically or using quantum chemistry methods.[5] For bonded systems, the residues of the MM part of the system are often subject to bond capping, and the QM and MM parts interface to approximations like atom in-linking.[6−10] Having defined the reference ground state in this way, the system can be the subject of time-dependent perturbation theory in terms of response functions, where the response (property or spectrum) of the system is defined and solved in the presence of all interactions.[2−4] This integrated multiscale approach including structure, dynamics, and properties of large atomically resolved systems have turned out to be very powerful for a wide range of application studies of extended systems and molecules in complex and/or confined environments, such as solutions, polymers, proteins, and DNA.[11−13]

So far, the multiscale integrated approaches have mostly been applied to organic embeddings, while organometallic, or pure metallic confinements, in terms of nanoparticles and surfaces, have been less attended. This is unfortunate from the point of view that metallic-assisted nanodevices show unique capabilities for a wide range of applications in modern sensing—in particular, single molecule sensing, in imaging and in energy conversion. While many of these applications rely on the plasmonic regime, there is certainly a call for theoretical structure−property design for metal containing nanodevices also operating outside the plasmonic regime and for which general embedding is necessary. For regular crystal surfaces, modern quantum mechanical codes implementing periodic conditions are available (for example, VASP[14] or SIESTA[15]), while, for the far more common cases of surfaces with broken symmetry or general nanostructured clusters, pure quantum approaches are not applicable other than for the smallest of such systems. The design of force fields for embedding using the integrated approach should take advantage of algorithms for systematic decomposition and fitting of charges and polarizabilities. Indeed, such force fields have been derived in works by Jensen et al. on noble metal embedding.[16−18] However, an obvious complication of metallic particle embedding is the almost-free motion of charges within the metallic cluster, and that the interaction with the QM shell should be regulated by "atomic capacitances" rather than by fixed charges, in addition

Received: October 15, 2013
Published: February 20, 2014

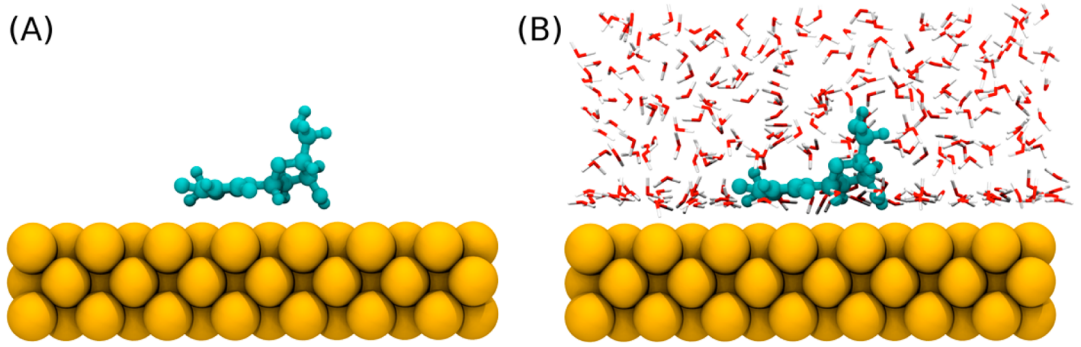

Figure 1. QM and MM regions partitioning in DFT/CMM approach: (A) molecule in QM region and metallic surface in MM region; (B) molecule in QM region and heterogeneous MM region separated into metallic surface part and nonmetallic part containing solvent molecules.

to polarizabilities. This notion was brought up by Jensen et al. in a work expressing capacitance−polarization model-derived force fields for metallic elements.[16] More recently, these authors applied the capacitance−polarizability model within the QM/MM approach for studies of optical properties of molecules on top of metal nanoparticles.[17−19] This effort can be viewed as bridging a gap between "small" and "large", where large nanoparticles commonly has been shown to be well-described using classical electrodynamics methods such as the Mie theory,[20] the discrete dipole approximation, and the finite difference time domain FDTD methods.[21,22] While these methods solve Maxwell's equations in continuous dieletric media without internal structure, the "small" approach using first-principles calculations, which solves all atomic and electronic structural degrees of freedom, are applicable to systems limited in size by up to a few hundred atoms. Thus, optical properties of real nanoparticle composites where an idealized continuum and an assumption of high symmetry does not hold call for approaches "in between", such as hybrid quantum classical models.

There are a few mainstream hybrid approaches that have been implemented to describe the optical properties of nanoparticles and nanoparticle−molecule composites, we refer here to Jensen and co-workers for a comprehensive account.[23] One is the polarizable continuum method of Corni and Tomasi,[24] who used a quantum mechanical description of the molecules but still retaining a (polarizable) continuum description of the nanoparticle; another is the heterogeneous solvation response theory of Jorgensen et al.,[25] where the quantum mechanical part of the system is described by a multiconfigurational self-consistent field. A variety of spectra and properties have been addressed by these methods. A few other models dealing with QM combined with FDTD have been proposed; in particular, Lopata and Neuhauser[26] combined FDTD electrodynamics with a two-state quantum approach and Masiello and Schatz[27] presented a continuum electrodynamics description of the metal combined with TD-DFT for the molecular property. Arcisaukaite et al.[28] used a polarizable QM/MM method to study the charge-transfer excitation energies of pyridine interacting with small silver clusters. Recently, Golze et al. extended conventional QM/MM approach by adding image charge effects and applied it to study adsorption processes at metallic interfaces.[29]

Here, we formulate a hybrid density functional theory/molecular mechanics (DFT/CMM) approach for molecular property calculations in heterogeneous environments, in which the metallic part of the environment is described by the capacitance−polarization model.[16−18,30,31] The model is generalized to different media environments, whereof, in particular, one metallic embedding and one solvent or organic embedding is an important example. This is the actual model for surface/nanoparticle adsorbates used for application in the present paper. In the following, we outline the DFT/CMM response theory, and the salient features of the theory, with respect to previous related works[17,18] and to conventional DFT/MM linear response theory.[2] We describe the technical aspects of the calculations and discuss results for the pyrimidine deoxynucleoside (thymidine) molecule on gold surfaces in aqueous solution, and then finalize the paper by making an outlook for further extensions and applications.

THEORY

The description of our DFT/CMM approach for evaluation of linear static and dynamic properties of molecules near metallic surfaces of arbitrary shape is organized in the following order: first, we describe the partitioning of the molecular system into quantum and classical regions; second, we introduce the capacitance−polarization model for heterogeneous MM regions; third, the Kohn−Sham method and linear response formalism is derived within the DFT/CMM approach, highlighting differences between our results and the ones obtained within a conventional DFT/MM approach.[2]

A. Partitioning of a Heterogeneous Molecular System in the DFT/CMM Approach. The first step of development of any QM/MM approach is the partitioning of the molecular system into distinct regions, which are described by quantum mechanical and classical methods. In conventional QM/MM approaches,[10,32,33] which are designed for treatment of predominantly organic systems like proteins or organic molecules in solvent environments, the separation of the QM and MM regions is well-defined (assuming absence of chemical bonds between the QM and MM regions): the QM region typically includes the molecule or molecular fragment of interest, while the MM region includes the remaining part of the system. Unfortunately, such a partitioning of the QM and MM regions cannot be directly assumed in the DFT/CMM approach, as the molecular system then is heterogeneous, i.e., consists of a metallic part (metal surface or nanoparticle) and a nonmetallic part (molecules). This heterogeneous nature of the full system instead imposes the following restrictions on its partitioning into QM and MM regions: (a) the QM region is selected from the nonmetallic part of the system; (b) the QM and MM regions must be selected in such way that strong chemical bonds between the QM region and the metallic part

of the MM region are avoided. These restrictions are not of fundamental nature, and can most probably be overcome in the future with the development of more-advanced quantum and classical mechanics methods. Taking these restrictions into account, our DFT/CMM approach is suitable for determination of linear properties of molecules physisorbed on metallic surfaces or metallic nanoparticles. More specifically, it is well suited for investigation of molecules "weakly" interacting with metallic surfaces or nanoparticles in vacuum and solvent environments (see Figure 1). Furthermore, the DFT/CMM approach can be applied to study also heterogeneous molecular systems, such as self-assembling monolayers on metal surfaces, provided the QM region is not involved in direct chemical bonding with the metal surface or nanoparticle. Thus, our DFT/CMM approach opens new possibilities for studying heterogeneous molecular systems, which are frequently encountered in various areas of surface science and nanoparticle research.

B. Capacitance−Polarization Model for Heterogeneous MM Region in the DFT/CMM Approach. The selection of a physically robust model for the heterogeneous MM region is a key factor determining the overall accuracy of the DFT/CMM approach. As it defines the nature and types of interactions included in the description of the interaction between the QM and MM regions, it ultimately determines which molecular systems can be treated within the approach. Here, following previous works by Jensen and co-workers,[17−19] we adopt, and further develop, a capacitance−polarization model-based description of the metallic part of the MM region. This model has a physically appealing description of the metallic surface or nanoparticle in terms of induced charges and dipoles, a verified good performance in modeling polarizabilities of nanoparticles,[16] and has well-parametrized force fields available for a few noble metals.[16] Thus, the heterogeneous MM part in the DFT/CMM approach is described using the following assumptions: (a) a capacitance−polarization model for electrostatics and polarization of the metallic part of the MM region; (b) distributed charges are used in the metallic part of the MM region and point charges are used in the nonmetallic part of the MM region; (c) van der Waals interaction between QM and MM atoms, as well as between atoms in the MM region, is modeled using an empirical Lennard-Jones potential. The outlined model of the heterogeneous MM region thus captures the essential physical features of a system consisting of molecules physisorbed on a metal surface or a nanoparticle in vacuum or in a solvent environment, and includes electrostatic, polarization, and van der Waals interactions between the molecules in the QM region, metal surface or nanoparticle in the MM region and solvent molecules in the MM region. Here, we would like to point out that the description of the nonmetallic part of the MM region is restricted to nonpolarizable force fields in our DFT/CMM approach due to pragmatic reasons, because the usage of polarizable force fields for this region would require the implementation of a self-consistent scheme for determination of induced charges/dipoles in the metallic part of the MM region and induced dipoles in the nonmetallic part of the MM region in both Kohn−Sham and density functional response codes. Jensen and co-workers[17−19] applied a capacitance−polarization model of this type to study optical properties of molecules absorbed on silver nanoparticles in vacuum within the time-dependent DFT formalism. Their results indicate that the capacitance−polarization model provides an adequate description of static and dynamic response from metallic nanoparticles to external electromagnetic fields, and makes computations of the metal surface or nanoparticle-induced shifts of molecular properties feasible.

The total energy of the complex system has several contributions within the DFT/CMM approach. Let us consider a system consisting of a single QM molecule physisorbed on an MM metal surface in a solvent environment (see Figure 1B). The total energy of this system can be written as[32]

$$E = E_{\mathrm{MM}} + E_{\mathrm{QM/MM}} + E_{\mathrm{QM}} \tag{1}$$

where the first term is the energy of the MM region, the second term is the interaction energy of the QM and MM regions, and the last term is the QM region energy, which, in our case, is obtained using the Kohn−Sham formalism. Using the above-described model for the heterogeneous MM region, which is the capacitance−polarization model[16,31] augmented with a nonpolarizable force field for nonmetallic part of MM region, the sum of the first two terms in eq 1 can be written as[17,18]

$$\begin{aligned} E_{\mathrm{QM}} + E_{\mathrm{QM/MM}} = {} & \frac{1}{2}\sum_{m,n\neq m} q_m^{\mathrm{ind}} T_{mn}^{qq} q_n^{\mathrm{ind}} - \frac{1}{2}\sum_{m,n\neq m} \mathbf{p}_m^{\mathrm{ind}} \mathbf{T}_{mn}^{pp} \mathbf{p}_n^{\mathrm{ind}} \\ & - \sum_{m,n\neq m} q_m^{\mathrm{ind}} \mathbf{T}_{mn}^{qp} \mathbf{p}_n^{\mathrm{ind}} + \frac{1}{2}\sum_m q_m^{\mathrm{ind}} c_m^{-1} q_m^{\mathrm{ind}} \\ & + \frac{1}{2}\sum_m \mathbf{p}_m^{\mathrm{ind}} \alpha_m^{-1} \mathbf{p}_m^{\mathrm{ind}} + \frac{1}{2}\sum_{m',n'\neq m'} q_{m'}^{\mathrm{perm}} T_{m'n'} q_{n'}^{\mathrm{perm}} \\ & + \sum_{m,n'} q_m^{\mathrm{ind}} T_{mn'}^{q} q_{n'}^{\mathrm{perm}} - \sum_{m,n'} \mathbf{p}_m^{\mathrm{ind}} \mathbf{T}_{mn'}^{p} q_{n'}^{\mathrm{perm}} \\ & + \sum_m q_m^{\mathrm{ind}} (\varphi_m^{\mathrm{ele}} + \varphi_m^{\mathrm{nuc}}) - \sum_m \mathbf{p}_m^{\mathrm{ind}} (\mathbf{E}_m^{\mathrm{ele}} + \mathbf{E}_m^{\mathrm{nuc}}) \\ & + \sum_{m'} q_{m'}^{\mathrm{perm}} (\varphi_{m'}^{\mathrm{ele}} + \varphi_{m'}^{\mathrm{nuc}}) + E_{\mathrm{MM}}^{\mathrm{vdW}} + E_{\mathrm{QM/MM}}^{\mathrm{vdW}} \end{aligned} \tag{2}$$

where the first five terms describe induced charge and induced dipole contributions to the energy of the metallic part of the MM region, and the sixth term describes the permanent charge contribution to the energy of nonmetallic part of the MM region. The seventh and eighth terms describe the interaction between metallic and nonmetallic parts of the MM region, the next three terms describe the interaction between charges and dipoles in the MM region and the QM region, and last two terms describe van der Waals interaction in the MM region and between MM and QM regions, respectively. More specifically, the first term in eq 2 describes the electrostatic interaction between the induced charges in the metallic part of the MM region; the second term describes the interaction between the induced dipoles in the metallic part of the MM region; the third term describes the interaction between the induced charges and induced dipoles in the metallic part of the MM region; the fourth and fifth terms describe the so-called induced charges and induced dipole self-energies, i.e., energies needed to create induced charges and induced dipoles at their positions in the metallic part of the MM region; the sixth term describes the interaction between permanent charges in the nonmetallic part of the MM region; the seventh and eighth terms describe the interaction between permanent charges in the nonmetallic part of the MM region with induced charges and induced dipoles in the metallic part of the MM region, respectively; the ninth and tenth terms describe interaction between induced charges and induced dipoles in the metallic part of the MM region and nuclei and electrons in the QM region; the eleventh term describes interaction between permanent charges in the

nonmetallic part of the MM region and nuclei and electrons in the QM region; the last two terms describe the van der Waals interaction in the MM region and between the QM and MM regions, respectively. In eq 2, we used the following notations: q_m^{ind} and $\mathbf{p}_m^{\mathrm{ind}}$ are the induced distributed charge and the induced distributed dipole at the mth atom in the metallic part of the MM region, respectively; T_{mn}^{qq}, $\mathbf{T}_{mn}^{qp}$, and $\mathbf{T}_{mn}^{pp}$ are the zero-, first-, and second-order electrostatic interaction tensors (see Appendix A); c_m is the capacitance of the mth atom in the metallic part of the MM region; α_m is the polarizability tensor of the mth atom in the metallic part of the MM region; φ_m^{ele} and φ_m^{nuc} are the potential created by electrons and nuclei in the QM region at the position of the mth atom in the metallic part of the MM region, respectively; $\mathbf{E}_m^{\mathrm{ele}}$ and $\mathbf{E}_m^{\mathrm{nuc}}$ are the electric field created by electrons and nuclei in the QM region at the position of the mth atom in the metallic part of the MM region, respectively; $q_{m'}^{\mathrm{perm}}$ is the permanent point charge at the m'th atom in the nonmetallic part of the MM region; $T_{m'n'}$ is the zero-order electrostatic interaction tensor between point charges (see Appendix A); $T_{mn'}^{q}$ and $\mathbf{T}_{mn'}^{p}$ are the zero- and first-order electrostatic interaction tensors between point charges and distributed charges and between point charges and distributed dipoles (see Appendix A); $\varphi_{m'}^{\mathrm{ele}}$ and $\varphi_{m'}^{\mathrm{nuc}}$ and are the potential created by electrons and nuclei in the QM region at the position of the m'th atom in the nonmetallic part of the MM region. The procedure for evaluation of the potential and electric field generated by nuclei and electrons at the various atom positions is described in Appendix A. From the definition of the MM region energy in eq 2, it is clear that the metallic MM region in this capacitance−polarization model is described by force fields defined via parametrized capacitances, isotropic polarizability tensors, and a set of Lennard-Jones parameters used for the van der Waals interaction potential. Jensen and Jensen, in their study of the capacitance-polarization model for metal nanoparticles, determined optimized values of capacitances and polarizabilities suitable for the modeling of gold and silver nanoparticles and surfaces.[16] We will use these force field parameters to describe the metallic MM region in our DFT/CMM calculations of the molecular properties.

The induced charges and dipoles in the metallic part of MM region can be determined by solving a linear set of equations[16−18,31]

$$\begin{pmatrix} \mathbf{A} & \mathbf{M} & \mathbf{0} \\ -\mathbf{M}^{\mathrm{T}} & -\mathbf{C} & \mathbf{1} \\ \mathbf{0} & \mathbf{1} & 0 \end{pmatrix} \begin{pmatrix} \mathbf{p}^{\mathrm{ind}} \\ \mathbf{q}^{\mathrm{ind}} \\ \lambda \end{pmatrix} = \begin{pmatrix} \mathbf{E}^{\mathrm{ele}} + \mathbf{E}^{\mathrm{nuc}} + \mathbf{E}^{\mathrm{perm}} \\ \mathbf{V}^{\mathrm{ele}} + \mathbf{V}^{\mathrm{nuc}} + \mathbf{V}^{\mathrm{perm}} \\ q^{\mathrm{tot}} \end{pmatrix} \tag{3}$$

where the first matrix is the so-called Relay matrix, which describes the coupling between induced charges and induced dipoles in the metallic part of the MM region; the second matrix is the collection of induced charges and induced dipoles in the metallic part of the MM region, and the Lagrangian multiplier λ, which imposes preservation of the total charge on the metallic part of the MM region; the third matrix is the collection of the potential and electric field created by the QM region and by the nonmetallic part of the MM region at the position of each atom in the metallic MM region and of the total charge q^{tot} on the metallic part of the MM region. In eq 3, induced charges $\{q_m^{\mathrm{ind}}\}$ and induced dipoles $\{p_m^{\mathrm{ind}}\}$ are collected into vectors $\mathbf{p}^{\mathrm{ind}}$ and $\mathbf{q}^{\mathrm{ind}}$; electric field and potential at positions of atoms in the metallic part of the MM region are collected into $(\mathbf{E}^{\mathrm{ele}} + \mathbf{E}^{\mathrm{nuc}} + \mathbf{E}^{\mathrm{perm}})$ and $(\mathbf{V}^{\mathrm{ele}} + \mathbf{V}^{\mathrm{nuc}} + \mathbf{V}^{\mathrm{perm}})$ vectors, which contain contributions from electrons and nuclei in the QM region and permanent charge in the nonmetallic part of the MM region, respectively.

The Relay matrix is defined by the distinct matrices **A**, **C**, and **M**, where the **A** matrix describes the interaction between the induced dipoles, the **C** matrix describes the interaction between induced charges, and the **M** matrix describes the interaction between induced dipoles and induced charges. The elements of these matrices have the following form:

$$\begin{aligned} \mathbf{A}_{mn} &= \alpha_m^{-1}\delta_{mn} - \mathbf{T}_{mn}^{pp}(1 - \delta_{mn}) \\ \mathbf{C}_{mn} &= c_m^{-1}\delta_{mn} + T_{mn}^{qq}(1 - \delta_{mn}) \\ \mathbf{M}_{mn} &= \mathbf{T}_{mn}^{qp}(1 - \delta_{mn}) \end{aligned} \tag{4}$$

Here, we used electrostatic interaction tensors of various orders, which are described in detail in Appendix A. The most straightforward way to determine the induced charges and induced dipoles from the set of linear equations described by eq 3 is to explicitly invert the Relay matrix. However, this approach is rarely used, since it becomes impractical for large metallic MM regions, and instead of explicitly constructing and inverting the Relay matrix for metallic MM regions of sizes exceeding a few thousand atoms, we use iterative procedures. We note that eq 3 reduces to the equation for determination of induced dipoles used in the conventional QM/MM methods if the induced charges are neglected and point charges instead of distributed charges are used in the description of the electrostatic interaction. This feature illustrates that the capacitance−polarization model for the MM region can be viewed as an advanced extension of conventional polarizable force field models for the MM region, which thus augments the previous QM/MM models with an inclusion of charge transfer between atoms in the MM region.

C. Determination of the Interaction Hamiltonian between the QM and MM Regions. The determination of the Hamiltonian terms, which describe the interaction between the QM and MM regions, has a trivial solution for molecular systems in which the MM region is described by a nonpolarizable force field, since, in this case, the interaction Hamiltonian is written as the sum of two terms: the first term describes the electrostatic interaction between electrons and nuclei in the QM region with permanent charges in the MM region, and the second term describes the van der Waals interaction between the QM and MM regions typically via an empirical potential. Unfortunately, already in conventional QM/MM methods, which use polarizable force fields, the form of the polarization term in the interaction Hamiltonian becomes nontrivial, as it explicitly includes a part of the MM Hamiltonian via the induced dipole moments.[32] The detailed discussion of this topic can be found in the work of Ahlström on polarizable force fields[34] and in later works[32] dealing with QM/MM methods with an MM region description at the polarizable force field level. In our case, the interaction Hamiltonian between the QM and MM regions can be defined in the following form:

$$\hat{H}_{\mathrm{QM/MM}} = \frac{1}{2}\sum_{m} q_m^{\mathrm{ind}}(\varphi_m^{\mathrm{ele}} + \varphi_m^{\mathrm{nuc}} + \sum_{m'} T_{mm'}^{q} q_{m'}^{\mathrm{perm}}) - \frac{1}{2}\sum_{m} \mathbf{p}_m^{\mathrm{ind}}(\mathbf{E}_m^{\mathrm{ele}} + \mathbf{E}_m^{\mathrm{nuc}} + \sum_{m'} \mathbf{T}_{mm'}^{p} q_{m'}^{\mathrm{perm}}) + \sum_{m'} q_{m'}^{\mathrm{perm}}(\varphi_{m'}^{\mathrm{ele}} + \varphi_{m'}^{\mathrm{nuc}}) + H_{\mathrm{QM/MM}}^{\mathrm{vdW}} \quad (5)$$

where the first term describes the interaction of induced charges in the metallic part of the MM region with electrons and nuclei in the QM region, as well as with permanent charges in the nonmetallic part of the MM region; the second term describes the interaction of induced dipoles in the metallic part of the MM region with electrons and nuclei in the QM region, as well as with permanent charges in the nonmetallic part of the MM region; the third term describes the interaction of permanent charges in the nonmetallic part of the MM region with electrons and nuclei in the QM region; the fourth term describes the van der Waals interaction between the MM and QM regions. Here, we point out that the procedure for evaluation of the potential generated by nuclei and electrons at atom positions in the metallic part of the MM region is different from the one used for its nonmetallic part (see Appendix A for details). From the above given expression of the interaction Hamiltonian $\hat{H}_{\mathrm{QM/QM}}$ for heterogeneous molecular systems, it is obvious that a strict separation of the MM region Hamiltonian from the interaction Hamiltonian between the QM and MM regions is not possible, as eq 5 includes coupling between induced charges and induced dipoles in the metallic part of the MM region with the potential and electric field generated by permanent charges in the nonmetallic part of the MM region. Thus, the nonmetallic and metallic parts of the MM region are coupled, and the molecular properties induced by heterogeneous environments in the DFT/CMM approach can therefore be computed using only the full model of the MM region. The simplified calculations in which one part of the MM region is neglected can potentially introduce large errors in estimations of the total environmental shifts of the molecular properties, because of strong coupling between the metallic and nonmetallic parts of the MM region. Here, we would also like to point out that the interaction Hamiltonian between QM and MM regions given by eq 5 reduces to the interaction Hamiltonian obtained by Jensen et al. for vacuum case, if contributions dependent on permanent charges in the nonmetallic part of the MM region are neglected in eqs 3 and 5.

D. Kohn–Sham Method within the DFT/CMM Approach. In the previous subsections, we outlined some details regarding the partitioning of a heterogeneous molecular system into QM and MM regions, and presented a capacitance–polarization model for the MM region which captures the main physical features of interactions between a metal surface or a nanoparticle and molecules in vacuum or in a solvent environment. Here, we employ these results to formulate the Kohn–Sham method for heterogeneous molecular systems within the DFT/CMM approach. We use the Kohn–Sham operator obtained in this subsection as the starting point for the derivation of the linear response formalism within the DFT/CMM approach.

We recall that the Kohn–Sham method in density functional theory is defined by its key component—the Kohn–Sham operator, which is used to obtain the Kohn–Sham orbitals in a self-consistent field scheme. This operator is determined by examining the minimization problem for the energy functional of the molecular system under an orthogonality constraint for the Kohn–Sham orbitals (see, for example, ref 1). Here, we apply the same procedure to the energy functional of the heterogeneous molecular system consisting of a QM region and a dual MM region with metallic and nonmetallic parts. As a first step in the determination of the Kohn–Sham operator, we define a Lagrangian for the energy functional as

$$\Omega(\{\phi_i\}, \varepsilon_{ij}) = E_{\mathrm{MM}} + E_{\mathrm{QM/MM}} + E_{\mathrm{QM}} + \varepsilon_{ij}(\langle\phi_i|\phi_j\rangle - \delta_{ij}) \quad (6)$$

where $E_{\mathrm{MM}} + E_{\mathrm{QM/MM}}$ is given by eq 2 for a dual metallic/nonmetallic MM region, (see Figure 1B). E_{QM} is the standard energy functional expression for the isolated QM region under vacuum, i.e.,

$$E_{\mathrm{QM}} = E_{\mathrm{kin}}[\rho(\mathbf{r})] + E_{\mathrm{col}}[\rho(\mathbf{r})] + E_{\mathrm{xc}}[\rho(\mathbf{r})] + E_{\mathrm{ext}}[\rho(\mathbf{r})] \quad (7)$$

ε_{ij} represents the Lagrangian multipliers for enforcement of orthogonality between the Kohn–Sham orbitals $\{\phi_i\}$, and $\langle\phi_i|\phi_j\rangle$ is the overlap integral between Kohn–Sham orbitals ϕ_i and ϕ_j. Here, we introduced four contributions to the energy functional of the QM region that are dependent on the electron density $\rho(\mathbf{r}) = \sum_i \phi_i^*(\mathbf{r})\phi_i(\mathbf{r})$ of which the first is the electron kinetic energy of the functional, the second term is the electron Coulomb interaction functional, the third term is the electron exchange-correlation functional, and the last term is the external potential functional, which, in this case, describes the Coulomb interaction between the electron density with the external potential. Taking a closer look at the structure of the energy functional Lagrangian of the molecular system, $\Omega(\{\phi_i\},\varepsilon_{ij})$, it is obvious that we can split the Kohn–Sham operator into two terms, as

$$\hat{H}_{\mathrm{KS}} = \hat{H}_{\mathrm{KS}}^{\mathrm{QM}} + \hat{H}_{\mathrm{KS}}^{\mathrm{QM/MM}} \quad (8)$$

where the first term is the ordinary Kohn–Sham operator of the isolated QM system under vacuum and the second term is an effective operator describing the interaction between the QM and MM regions. Both terms in the above equation are obtained by variation of $\Omega(\{\phi_i\},\varepsilon_{ij})$, where the first term arises from variation of E_{QM} and the second term arises from variation of $E_{\mathrm{MM}} + E_{\mathrm{QM/MM}}$. Using the formalism of second quantization, $\hat{H}_{\mathrm{KS}}^{\mathrm{QM}}$ is defined as

$$H_{\mathrm{KS}}^{\mathrm{QM}} = f_{pq}^{\mathrm{QM}}\hat{E}_{pq} = \left\langle \phi_p \middle| -\frac{1}{2}\nabla^2 + \int \frac{\rho(\mathbf{r}')}{|\mathbf{r}-\mathbf{r}'|}\,\mathrm{d}\mathbf{r}' + \frac{\delta E_{xc}[\rho(\mathbf{r})]}{\delta\rho(\mathbf{r})} - \sum_N \frac{Z_N}{|\mathbf{r}-\mathbf{R}_N|} \middle| \phi_q \right\rangle \hat{E}_{pq} \quad (9)$$

where the matrix element f_{pq}^{QM} is separated into four contributions, according to eq 7, and $\hat{E}_{pq}$ is the standard single particle excitation operator. Here, we introduced two new quantities in the definition of the external potential term, namely, the charge Z_N and the position vector $\mathbf{R}_N$ of the Nth nucleus in the QM region. The determination of $\hat{H}_{\mathrm{KS}}^{\mathrm{QM/MM}}$ is a more challenging task that requires some tedious algebraic manipulations that exploit the structure of eq 2. Here, we omit these details and provide the final results obtained for the two types of MM regions considered in this work. For the

heterogeneous MM region (see Figure 1B), $\hat{H}_{\mathrm{KS}}^{\mathrm{QM/MM}}$ can be written as

$$\begin{aligned}\hat{H}_{\mathrm{KS}}^{\mathrm{QM/MM}} &= f_{pq}^{\mathrm{QM/MM}}\hat{E}_{pq} \\ &= \langle\phi_p|\sum_m q_m^{\mathrm{ind}}\hat{T}_m^q(\mathbf{r}) - \sum_m \mathbf{p}_m^{\mathrm{ind}}\hat{\mathbf{T}}_m^p(\mathbf{r}) \\ &\quad - \sum_{m'} q_{m'}^{\mathrm{perm}}\hat{T}_{m'}(\mathbf{r})|\phi_q\rangle\hat{E}_{pq}\end{aligned} \tag{10}$$

where the first term describes electrons in the QM region interacting with induced charges in the metallic part of the MM region and the second term describes electrons in the QM region interacting with induced dipoles in the metallic part of the MM region, and the third term describes electrons in the QM region interacting with permanent charges in the nonmetallic part of the MM region. Here, we introduced the potential operators, $\hat{T}_m^q(\mathbf{r})$ and $\hat{T}_{m'}(\mathbf{r})$, and the electric field operator, $\hat{\mathbf{T}}_m^p(\mathbf{r})$, the definitions of which can be found in Appendix A. The given expression for $\hat{H}_{\mathrm{KS}}^{\mathrm{QM/MM}}$ resembles the one obtained in the DFT/MM/PCM method[4] and is closely related to it. Comparing the above given expression for $\hat{H}_{\mathrm{KS}}^{\mathrm{QM/MM}}$ with the one used in the conventional DFT/MM approach with polarizable force fields,[2] two major differences can be noted. First, we have contributions of additional induced charges due to the use of the capacitance−polarization model to describe the pure metallic MM region. Second, the potential and electric field operators used in the DFT/CMM approach are inherently damped by the distributed nature of the induced charges and induced dipoles. Furthermore, the conventional QM/MM approach can be considered as a limiting case of our DFT/CMM approach, as the contribution due to the induced dipoles to the Kohn−Sham operator in that approach can be obtained from eq 10 by setting the capacitance for each MM atom to zero and replacing the distributed dipoles with point dipoles, and neglecting permanent charge contributions from the nonmetallic part of the MM region.

From a practical point of view, the implementation of the DFT/CMM approach poses a considerably more complex undertaking compared to the conventional QM/MM approach, as the one-electron integrals required for evaluation of matrix elements entering eq 10 are not readily available in quantum chemistry programs. In Appendix B, we provide a description of an implementation of these integrals using the McMurchie−Davidson scheme.[35]

Taking a closer look at the $\hat{H}_{\mathrm{KS}}^{\mathrm{QM/MM}}$ for the heterogeneous MM region (Figure 1B), we can make the following conclusions. The nonmetallic MM region will influence the electron density of the QM region in a way similar to the other external potentials, such as the nuclei in the QM region considered here. However, the term in $\hat{H}_{\mathrm{KS}}^{\mathrm{QM/MM}}$ that is dependent on induced charges and induced dipoles, is also explicitly dependent on the electron density in the QM region and thus behaves similarly to the electron Coulomb interaction term in $\hat{H}_{\mathrm{KS}}^{\mathrm{QM}}$ of the Kohn−Sham operator. Thus, these two terms will play an important role in the linear response formalism for the DFT/CMM approach, which is described in the next subsection.

E. Linear Response Formalism within the DFT/CMM Approach. In the previous subsection, we introduced the Kohn−Sham method within the DFT/CMM approach, which is suitable for the calculation of electronic structure of the QM region in heterogeneous molecular systems in which the MM region is of the considered pure metallic or dual metallic/nonmetallic nature. As in this work, we are primarily interested in computations of optical and magnetic properties in heterogeneous molecular systems; we need to go beyond the Kohn−Sham method and implement a linear response formalism within the DFT/CMM approach—a formalism that allows for computation of arbitrary molecular properties defined using linear response functions or their residues.

Over the past decade, the response theory methods, including linear, quadratic, and cubic response formalisms, have been implemented in DFT[36−39] and hybrid DFT/MM settings.[2] The majority of these implementations have been based either on Ehrenfest's principle or the quasi-energy approach.[37] Here, we adopt the former methodology to formulate a linear response theory for the DFT/CMM approach, and we make use of it to determine the time evolution of the electron density in the QM region in heterogeneous molecular systems. We first define, following our previous works on linear response theory in DFT,[37,38] the time-dependent Kohn−Sham equations for the time evolution of the Kohn−Sham determinant:

$$\hat{H}_{\mathrm{KS}}(t) + \hat{V}(t)|\tilde{0}\rangle = i\frac{\mathrm{d}}{\mathrm{d}t}|\tilde{0}\rangle \tag{11}$$

Here, $\hat{H}_{\mathrm{KS}}(t)$ is the time-dependent Kohn−Sham operator, $\hat{V}(t)$ is the time-dependent perturbation acting on the QM region, and $|\tilde{0}\rangle$ is the time-dependent Kohn−Sham determinant, which is parametrized using an exponential ansatz, i.e.,

$$|\tilde{0}\rangle = \exp[-\kappa(t)]|0\rangle \tag{12}$$

Here, in the last equation, we introduced the anti-Hermitian time evolution operator $\hat{\kappa}(t)$, which is defined as

$$\hat{\kappa}(t) = \sum_{pq}\kappa_{pq}(t)\hat{E}_{pq} \tag{13}$$

using the set of time-dependent Kohn−Sham orbital rotation parameters $\{\kappa_{pq}(t)\}$, and the Kohn−Sham determinant $|0\rangle$ of the unperturbed QM system, which is constructed from the set of orbitals $\{\phi_p\}$. Also, in eq 11, we introduced the time-dependent Kohn−Sham operator for a heterogeneous system, which is obtained in the same way as the Kohn−Sham operator described in the previous subsection (see eq 8), just instead of the electron density $\rho(\mathbf{r})$ of the unperturbed QM region, the time-dependent electron density $\rho(\mathbf{r},t)$ of the QM region is then considered. Taking into account the exponential parametrization of the Kohn−Sham determinant, the time-dependent electron density of the QM region can be written as

$$\rho(\mathbf{r}, t) = \langle 0|\exp[\hat{\kappa}(t)]\hat{\rho}(\mathbf{r})\exp[\hat{\kappa}(t)]|0\rangle \tag{14}$$

where we explicitly inserted the exponential time evolution operator for the Kohn−Sham determinant (see eq 12) and introduced the so-called electron density operator in its second quantitized form, i.e.,

$$\hat{\rho}(\mathbf{r}) = \sum_{pq}\phi_p^*(\mathbf{r})\phi_q(\mathbf{r})\hat{E}_{pq} \tag{15}$$

After this recapitulation of the basic quantities and operators appearing in response theory, we move directly to the derivation of linear response equations for the DFT/CMM approach. We then first apply Ehrenfest's principle to determine the time-dependent parameters $\{\kappa_{pq}(t)\}$, which define time evolution of electron density of the QM region.

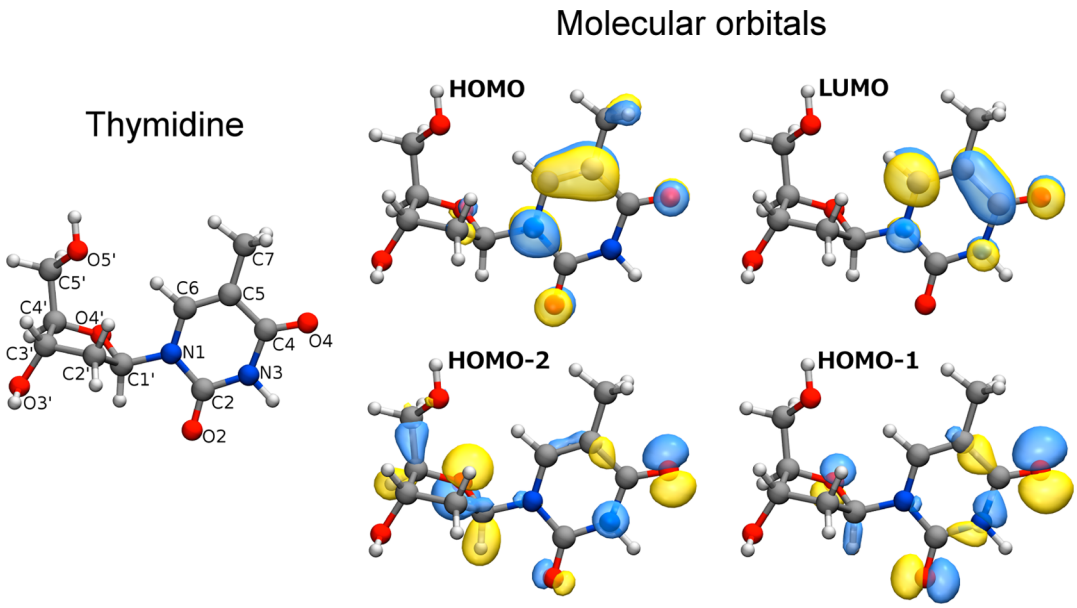

Figure 2. Thymidine molecule and its frontier molecular orbitals. Standard coloring scheme is used for the molecule: oxygens are red, nitrogens are blue, carbons are gray, and hydrogens are white.

As has been shown in our previous works, the Ehrenfest's principle can be expressed in the following set of equations:

$$\left\langle 0\middle|\left[\hat{Q},\ \exp(\kappa(t))\left(\hat{H}_{\mathrm{KS}}(t)+\hat{V}(t)-i\frac{\mathrm{d}}{\mathrm{d}t}\right)\exp(-\kappa(t))\right]\middle|0\right\rangle = 0 \tag{16}$$

where we introduced the arbitrary operator $\hat{Q}$, which will later be replaced by single-particle excitation and de-excitation operators. In order to arrive at the linear response equations from eq 16, we need to expand the time evolution operator into orders of perturbation, i.e., $\hat{\kappa}(t) = \hat{\kappa}^{(1)}(t) + \hat{\kappa}^{(2)}(t) + \hat{\kappa}^{(3)}(t) + \cdots$, and retain only the first-order term in eq 16, and carry out a Fourier transformation of all quantities involved from the time to the frequency domain. For a detailed description of these steps, we refer to basic articles on response theory for DFT.[36−39] The final result, in terms of linear response equations, reads

$$\langle 0|[\hat{\mathbf{q}},\ [\hat{\kappa}^{\omega},\ \hat{H}^{0}_{\mathrm{KS}}] + H^{\omega}_{\mathrm{KS}}]|0\rangle + \omega\langle 0|[\hat{\mathbf{q}},\ \hat{\kappa}^{\omega} - \hat{V}^{\omega}]|0\rangle = 0 \tag{17}$$

where H^{0}_{KS} is the Kohn−Sham operator of the unperturbed QM region in the heterogeneous molecular system (see eqs 8−10). Here, H^{ω}_{KS} is the first order contribution to the Kohn−Sham operator of the perturbed QM region in the frequency domain, $\hat{\kappa}^{\omega}$ is first order contribution to the time evolution operator $\hat{\kappa}(t)$ in the frequency domain, $\hat{V}^{\omega}$ is an external perturbation operator in the frequency domain, and $\hat{\mathbf{q}}$ is the column vector of one-particle excitation operators (see ref 37 for details). Recalling the given definition of the Kohn−Sham operator in the previous subsection, the only quantity that remains undefined is the $\hat{H}^{\mathrm{QM/MM},\omega}_{\mathrm{KS}}$ term in H^{ω}_{KS}, which describes the interaction between the QM and MM regions due to the first-order perturbed density of the QM region, i.e., $\rho^{\omega}(\mathbf{r}) = \sum_{pq}\phi^{*}_{p}(\mathbf{r})\phi_{q}\langle 0|\,[\kappa^{\omega},\ \hat{E}_{pq}]\,|0\rangle$. Using the same procedure as that which we employed to find the Kohn−Sham operator of an isolated heterogeneous molecular system, we obtain the following expression for $\hat{H}^{\mathrm{QM/MM},\omega}_{\mathrm{KS}}$:

$$\begin{aligned} H^{\mathrm{QM/MM},\omega}_{\mathrm{KS}} &= f^{\mathrm{QM/MM},\omega}_{pq}\hat{E}_{pq} \\ &= \langle\phi_p|\sum_m q^{\mathrm{ind},\omega}_m \hat{T}^{q}_m(\mathbf{r}) - \sum_m \mathbf{p}^{\mathrm{ind},\omega}_m \hat{\mathbf{T}}^{p}_m(\mathbf{r})|\phi_q\rangle\hat{E}_{pq} \end{aligned} \tag{18}$$

where $q^{\mathrm{ind},\omega}_m$ and $\mathbf{p}^{\mathrm{ind},\omega}_m$ are the induced charges and induced dipoles in the metallic MM region, because of the first-order perturbed density in the QM region. These charges and dipoles are evaluated by solving the following set of linear equations:

$$\begin{pmatrix} \mathbf{A} & -\mathbf{M} & 0 \\ -\mathbf{M}^{\mathrm{T}} & -\mathbf{C} & 1 \\ 0 & 1 & 0 \end{pmatrix}\begin{pmatrix} \mathbf{p}^{\mathrm{ind},\omega} \\ \mathbf{q}^{\mathrm{ind},\omega} \\ \lambda \end{pmatrix} = \begin{pmatrix} \mathbf{E}^{\mathrm{ele},\omega} \\ \mathbf{V}^{\mathrm{ele},\omega} \\ q^{\mathrm{tot}} \end{pmatrix} \tag{19}$$

where the expressions for the electric field and potential vector dependent on the first-order perturbed density in the QM region is given in Appendix A. Here, we emphasize that the first-order contribution to the Kohn−Sham operator of the perturbed heterogeneous molecular system involves only coupling between the metallic part of the MM region and the QM region. Furthermore, differently from conventional QM/MM methods with polarizable force fields, the contributions appear not only from induced dipoles, but also from induced charges in our case.

Before concluding the presentation of the linear response formalism within the DFT/CMM approach, we inspect more closely how the metallic and nonmetallic parts of the MM region interact with the QM region in the prospective of the linear response equations. We note that the description model for the MM region used in this work does not allow for inclusion of direct interactions due to external perturbations with the MM region and, in particular, with its metallic part. Thus, plasmonic effects as well as electromagnetic field reflection effects from the surface are not included in the DFT/CMM approach in its current form. Here, we also note that our model for the MM region within our DFT/CMM approach is able to describe the coupling between the metallic and nonmetallic parts of the MM system at the level of the

unperturbed system, and that the contributions to the linear response equations that explicitly depend on the perturbed electron density of the QM region is obtained only from the metallic part of the MM region. This limitation can be resolved by using polarizable force fields to describe the nonmetallic part of the QM region; however, so far, no such force fields have been developed in combination with the capacitance−polarization model for the metallic part of the MM region. Thus, efforts in force field construction are needed to overcome this limitation of the DFT/CMM approach.

■ COMPUTATIONAL DETAILS

We select thymidine as the adsorbent on a gold surface to test the performance of the DFT/CMM approach for description of molecular properties in heterogeneous environments, because of the fact that the interaction between thymidine and gold has been investigated by experiments[40] and theoretical calculations[41] and that gold nanoparticles capped by thymidine have been shown to be able to cross intracellular barriers.[42] Here, we study the lowest excited states of thymidine (see Figure 2) physisorbed on two different gold surfaces, Au(100) and Au(111), under vacuum and in an aqueous environment. For both surfaces, 100 snapshots of the thymidine adsorbate on gold surface have been extracted from molecular dynamic (MD) simulations, applying subsequently the DFT/CMM approach to study two lowest excited states of these conformations of the adsorbates. In the following, we briefly describe details of MD simulations and DFT/CMM calculations.

A. Molecular Dynamics Simulations. Molecular dynamics simulations were carried out for one thymidine molecule adsorbed onto Au(100) and Au(111) surfaces under vacuum and in aqueous solution. The CHARMM22 force field[43,44] and the TIP3P-CHARMM model[43] were adopted to describe the thymidine molecule and water molecules, respectively, while the GolP-CHARMM force field[45] was used to model the gold surfaces. A remarkable advantage of the GolP-CHARMM force field is that the image charge effect on the gold surface is taken into account by an ensemble of rigid rods, which impose a small dipole on each Au atom. Another feature of the GolP-CHARMM force field is that the surface layer of Au atoms is furnished with virtual interacting sites, which ensures the correct adsorbing site and retains the simplicity of the Lennard-Jones potential. For the Au(100) and Au(111) surfaces, the area of the gold slab is set to 32.63 Å × 32.63 Å and 34.98 Å × 34.62 Å, corresponding to 128 and 168 Au atoms per layer, respectively. Six layers were employed to model each slab. The z-dimension of the simulation cell was set to 73.41 Å for Au(100) and 70.67 Å for Au(111), respectively, and periodic boundary conditions were applied along the three dimensions.

Four systems were simulated, i.e., thymidine on Au(100) under vacuum, aqueous thymidine on Au(100), thymidine on Au(111) under vacuum, and aqueous thymidine on Au(111). The initial structures for the MD simulations were created by putting a thymidine molecule above the gold surface with a vertical distance of ∼8 Å. During the pre-equilibrium simulations, the thymidine molecule spontaneously approached the gold surface, except for the case of aqueous thymidine on the Au(100) surface. Reducing the initial distance between thymidine and gold surface to 6 Å did not provide a stable adsorbed structure; thus, we adopted the structure of thymidine adsorbed on Au(100) under vacuum (∼3.7 Å above the gold surface) as the starting conformation of simulations for the aqueous environment.

All MD simulations were carried out using the GROMACS program package,[46] employing a constant-NVT ensemble with temperature maintained at 298 K using the stochastic velocity rescaling (v-rescale) algorithm,[47] that is an improved version of the Berendsen temperature coupling method that produces a correct canonical ensemble. For each system, the simulation was performed for 10 ns with a time step of 1 fs. During the simulations, the Lennard-Jones potential accounting for van der Waals interactions was smoothly switched to zero within 11−12 Å, and the Coulombic interaction was treated by the particle-mesh Ewald summation approach[48,49] with a real space cutoff at 12 Å and a Fourier spacing of 1.2 Å in the reciprocal space.

B. DFT/CMM Calculations of Excitation Energies. Based on snapshots extracted from the MD simulations, subsequent DFT/CMM calculations were carried out with the thymidine molecule described at the DFT level, and with the gold slab described by the frequency-independent capacitance−polarization model (gold capacitance has been set to 1.2159 and gold polarizability has been set to 39.5297, according to recommendations in the works by Jensen and co-workers[16−18,23]), and with the water molecules treated by the conventional TIP3P force field,[50] using a development version of the DALTON quantum chemistry program suite.[51] Since the DFT/CMM method in this work is developed to deal with nonperiodic systems, the gold surface was represented by a truncated cylinder with three layers of Au atoms. Different truncation radii were tested, and it was found that under physisorption the truncation radius introduces negligible effect on the computed absorption spectra of the adsorbent as long as it is larger than 10 Å. For production calculations, a truncation radius of 15 Å was used. For thymidine, the hybrid PBE0 functional[52] was employed together with the TZVP basis set,[53] and the linear response DFT/CMM calculations were carried out to obtain excitation energies and oscillator strengths of the lowest singlet excited states.

■ RESULTS AND DISCUSSION

To illustrate the capacity and indicate what type of information one can extract from our developed DFT/CMM linear response method, we show results from a study of thymidine on two different gold surfaces, Au(100) and Au(111), under vacuum and in aqueous solution. In the following, we discuss the absorption spectrum referring to the lowest excited states of the free thymidine molecule, and changes in the spectra induced by thymidine physisorption on the Au(100) or Au(111) surfaces under vacuum and in aqueous solution.

A. Lowest Excited States in Thymidine. We first examined free thymidine using a DFT linear response method at the PBE0[52]/TZVP[53] level; the results are listed in Table 1. The first excited state S_1 is a typical $n\pi^*$ excited state with an excitation energy of 4.91 eV, in accordance with previously reported TD-DFT results of thymine (4.87 eV; see the work by Gustavsson et al.[54]). The S_1 state corresponds to electron excitation from the lone-pair orbital of the carbonyl group (HOMO-1, see Figure 2) to the π^* orbital of the thymine ring (LUMO, see Figure 2) and exhibits a very small oscillator strength that cannot be observed in the experimental spectrum. The second excited state S_2 of thymidine is of the $\pi\pi^*$ type and corresponds to excitation from a π-type HOMO orbital to a π^*-type LUMO orbital (see Figure 2). This excitation has large

dx.doi.org/10.1021/ct400897s | J. Chem. Theory Comput. 2014, 10, 989−1003

Table 1. Computed Excitation Energies (E_{exc}), Oscillator Strengths (f), and MO Compositions for the Low-Lying Singlet Excitations of Thymidine under Vacuum

excited state[a]	E_{exc} (eV)	f	MO composition
S_1	4.907	0.004	H-1 → L (79%)
			H-2 → L (12%)
S_2	5.055	0.217	H → L (91%)
S_3	5.910	0.005	H-1 → L (16%)
			H-2 → L (74%)

[a]The excited states of thymidine are computed at the TD-PBE0/def-TZVP level of theory.

transition moment and dominates the UV/vis absorption spectrum. The excitation energy of the S_2 state is computed as 5.06 eV, in agreement with a previous TD-DFT study of thymine under vacuum (5.06 eV; see the work of Gustavsson et al.[54]) Compared with the experimentally measured absorption peak of thymine in aqueous solution (4.68 eV, see the work of Gustavsson et al.[54]), the computed excitation energy for the $\pi\pi^*$ transition shows a small blue shift due to the neglect of solvent effects and because of the method, which tends to overstabilize the π-bonding orbital.[54] The third excited state S_3 of thymidine is similar to the S_1 state of $n\pi^*$ type. It corresponds to a dominant excitation from the lone pair localized on oxygen O4′ in the sugar group to the π^*-type LUMO on the thymidine ring, instead of excitation from the oxygen lone pair on carboxyl to the π^*-type LUMO on thymidine ring, such as that in the S_1 state. Not surprisingly, the oscillator strength of the S_3 state is very small, being of similar magnitude to that of the S_1 state. Overall, the UV/vis absorption of thymidine is dominated by its S_2 state, and out of the $n\pi^*$-type excited states described here, only S_1 is in the proximity of S_2 and can borrow intensity from the S_2 state via electronic-vibrational coupling. Taking this into account, we consider only the first two excited states of thymidine in the following discussion of the lowest excited states of thymidine adsorbates on gold surfaces.

B. Thymidine on Gold Surfaces. To verify that the CHARMM force field can appropriately reproduce the geometry of the thymidine molecule, we compared the optimized geometries from DFT calculations at the B3LYP/def-TZVP level of theory and from energy minimization by force field. The comparison suggests that the deviation between QM and MM geometries arises mainly from rotation of the methyl group, and the obtained root-mean-square deviation (RMSD) is 0.175 Å for the whole molecule and 0.090 Å excluding all hydrogen atoms. MD simulations show that the thymidine molecule adopts different conformations on the Au(100) and the Au(111) surfaces. To reasonably account for the thermodynamic motions of thymidine, we evenly extracted 100 snapshots from the last 5-ns trajectories of the two systems (thymidine on Au(100) and thymidine on Au(111)). These snapshots were fed into subsequent linear response DFT/CMM calculations of the low-lying excited states of the thymidine molecule. For each system, the computed excitation energies, oscillator strengths, and molecular orbital (MO) compositions of the two lowest excited singlet states were averaged over 100 snapshots. The results are listed in Tables 2 and 3. It can be seen that even in the absence of gold surfaces the excitation energies of thymidine are subject to red-shift,

Table 2. Averaged Excitation Energies (E_{exc}) with Standard Deviations in Parentheses, Oscillator Strengths (f), and MO Compositions for the Low-Lying Singlet Excitations of Thymidine on the Au(100) Surface

system[a]	excited state[b]	E_{exc} (eV)	f	MO composition
dT only	S_1	4.693 (0.151)	0.020	H → L (10%)
				H-1 → L (80%)
	S_2	4.913 (0.108)	0.208	H → L (84%)
				H-1 → L (10%)
dT + Au(100)	S_1	4.732 (0.133)	0.115	H → L (40%)
				H-1 → L (52%)
	S_2	4.867 (0.112)	0.175	H → L (56%)
				H-1 → L (35%)

[a]"dT" denotes the thymidine molecule. [b]The excited states of thymidine are computed by DFT/CMM linear response formalism at the PBE0/def-TZVP level of theory and averaged over 100 snapshots.

Table 3. Averaged Excitation Energies (E_{exc}) with Standard Deviations in Parentheses, Oscillator Strengths (f), and MO Compositions for the Low-Lying Singlet Excitations of Thymidine on the Au(111) Surface

system[a]	excited state[b]	E_{exc} (eV)	f	MO composition
dT only	S_1	4.676 (0.183)	0.027	H → L (13%)
				H-1 → L (77%)
	S_2	4.923 (0.140)	0.193	H → L (81%)
				H-1 → L (11%)
dT+Au(111)	S_1	4.724 (0.160)	0.124	H → L (44%)
				H-1 → L (45%)
	S_2	4.877 (0.151)	0.162	H → L (52%)
				H-1 → L (33%)

[a]"dT" denotes the thymidine molecule. [b]The excited states of thymidine are computed by DFT/CMM linear response formalism at the PBE0/def-TZVP level of theory and averaged over 100 snapshots.

because of thermal fluctuation in the structure of the molecule, compared to that of the optimized thymidine molecule (see Table 1). The inclusion of gold surfaces in the DFT/CMM calculations give further rise to a red-shift in the excitation energy for S_2 and a blue-shift in the excitation energy for S_1, and such effects are of similar magnitude for the Au(100) and Au(111) surfaces. However, the two gold surfaces have different effects on the structure of excitations, namely, the MO compositions. The original S_1 state of the thymidine molecule in the absence of gold surfaces consists of 77%−80% HOMO-1 → LUMO transition and 10%−13% HOMO → LUMO transition. Note that the presence of the Au(111) surface results in a significant mixing between HOMO-1 → LUMO and HOMO → LUMO in the S_1 state with proportions of 45% and 44%, respectively (see Table 3). The oscillator strength of S_1 is, in turn, notably enhanced. Moreover, the S_2 state of thymidine on Au(111) surface also features mixing between HOMO-1 → LUMO and HOMO → LUMO transitions, and the oscillator strength decreases due to an increased proportion of the HOMO-1 → LUMO transition, which is of $n\pi^*$ character. The presence of the Au(100) surface led to less-pronounced variations in the MO compositions of

the S_1 and S_2 states compared to the Au(111) surface, resulting in slightly smaller effects on the oscillator strengths (Table 2). Thus, linear response DFT/CMM calculations suggest that the presence of gold surfaces (especially the Au(111) surface) enhances the proportions of the HOMO → LUMO transition in the S_1 state and the HOMO-1 → LUMO transition in the S_2 state, which, in turn, leads to a red-shifted absorption spectrum with an enhanced oscillator strength of the S_1 state.

C. Thymide on Gold in an Aqueous Environment. The aqueous environment enhances the difference in the effects of the two gold surfaces. As shown in Table 4, the inclusion of both the Au(100) surface and the water environment leads to an enhanced oscillator strengths of the S_1 state and a diminished oscillator strength of the S_2 state, together with changes in their corresponding MO compositions. DFT/MM calculations on the subsystem thymidine + water suggest that the presence of water molecules gives rise to blue-shifted excitation energies for both S_1 and S_2 states and a diminished oscillator strength for the S_2 state. However, the presence of the Au(100) surface tends to enhance the oscillator strength for the S_2 state, despite the fact that the proportion of the HOMO → LUMO transition in the S_2 state is smaller than that for thymidine under vacuum (Table 4). The overall effects of the Au(100) surface and water molecules lead to a partial mixing between the S_1 and S_2 states with blue-shifted excitation energies, an enhanced oscillator strength for the S_1 state and a diminished oscillator strength for the S_2 state. However, the inclusion of both water and the Au(111) surface in the DFT/CMM calculations leads to a more significant reversal in the structure of the original S_1 and S_2 states (Table 5), where the S_1 state consists of a major proportion of the HOMO → LUMO transition (70%) and a minor proportion of the HOMO → LUMO transition (21%). The oscillator strength for the S_1 state hence receives huge enhancement and becomes as large as 0.196. Consequently, the oscillator strength for the S_2 state becomes much smaller due to a significant increase in the proportion of the HOMO−1 → LUMO and HOMO−2 → LUMO transitions, which contribute little to the oscillator strength. Separate calculations on the two subsystems (thymidine + Au(111) and thymidine + water) suggest that the presence of the Au(111) surface leads to significant mixing between HOMO → LUMO and HOMO−1 → LUMO

Table 4. Averaged Excitation Energies (E_{exc}) with Standard Deviations in Parentheses, Oscillator Strengths (f), and MO Compositions for the Low-Lying Singlet Excitations of Thymidine on Aqueous Au(100) Surface

system[a]	excited state[b]	E_{exc} (eV)	f	MO composition
dT	S_1	4.626 (0.188)	0.019	H → L (12%)
				H-1 → L (70%)
	S_2	4.911 (0.154)	0.187	H → L (82%)
				H-1 → L (9%)
dT + Au(100)	S_1	4.684 (0.176)	0.071	H → L (29%)
				H-1 → L (47%)
				H-2 → L (16%)
	S_2	4.886 (0.157)	0.193	H → L (66%)
				H-1 → L (15%)
				H-2 → L (11%)
dT + H_2O	S_1	4.837 (0.178)	0.069	H → L (35%)
				H-1 → L (51%)
	S_2	5.053 (0.163)	0.141	H → L (59%)
				H-1 → L (24%)
dT + Au(100) + H_2O	S_1	4.848 (0.166)	0.151	H → L (57%)
				H-1 → L (30%)
	S_2	5.050 (0.174)	0.118	H → L (38%)
				H-1 → L (35%)
				H-2 → L (12%)

[a]"dT" denotes the thymidine molecule. [b]The excited states of thymidine are computed by DFT/CMM linear response formalism at the PBE0/def-TZVP level of theory and averaged over 100 snapshots.

Table 5. Averaged Excitation Energies (E_{exc}) with Standard Deviations in Parentheses, Oscillator Strengths (f), and MO Compositions for the Low-Lying Singlet Excitations of Thymidine on Aqueous Au(111) Surface

system[a]	excited state[b]	E_{exc} (eV)	f	MO composition
dT	S_1	4.680 (0.164)	0.031	H → L (17%)
				H-1 → L (72%)
	S_2	4.908 (0.117)	0.186	H → L (78%)
				H-1 → L (14%)
dT + Au(111)	S_1	4.703 (0.155)	0.098	H → L (37%)
				H-1 → L (51%)
	S_2	4.873 (0.118)	0.180	H → L (59%)
				H-1 → L (28%)
dT + H_2O	S_1	4.822 (0.148)	0.117	H → L (54%)
				H-1 → L (35%)
	S_2	5.036 (0.160)	0.100	H → L (40%)
				H-1 → L (33%)
				H-2 → L (11%)
dT + Au(111) + H_2O	S_1	4.810 (0.139)	0.196	H → L (70%)
				H-1 → L (21%)
	S_2	5.038 (0.170)	0.083	H → L (25%)
				H-1 → L (44%)
				H-2 → L (15%)

[a]"dT" denotes the thymidine molecule. [b]The excited states of thymidine are computed by DFT/CMM linear response formalism at the PBE0/def-TZVP level of theory and averaged over 100 snapshots.

dx.doi.org/10.1021/ct400897s | J. Chem. Theory Comput. 2014, 10, 989−1003

transitions in the S_1 state, and that water molecules resulted in an even-higher percentage of the HOMO → LUMO transition in the S_1 state (54%, see Table 5). The overall effects of the Au(111) surface and water molecules lead to a reversal of the S_1 and S_2 states, both with blue-shifted excitation energies. It is noteworthy that the presence of water molecules on both gold surfaces significantly lifted the excitation energies. The gold surfaces put sizable effects on the oscillator strengths; however, their effects on the excitation energies are much smaller, compared with those of a water environment.

The charge distributions on gold surfaces are shown in Figures 3 and 4, where the charge densities are obtained as two-

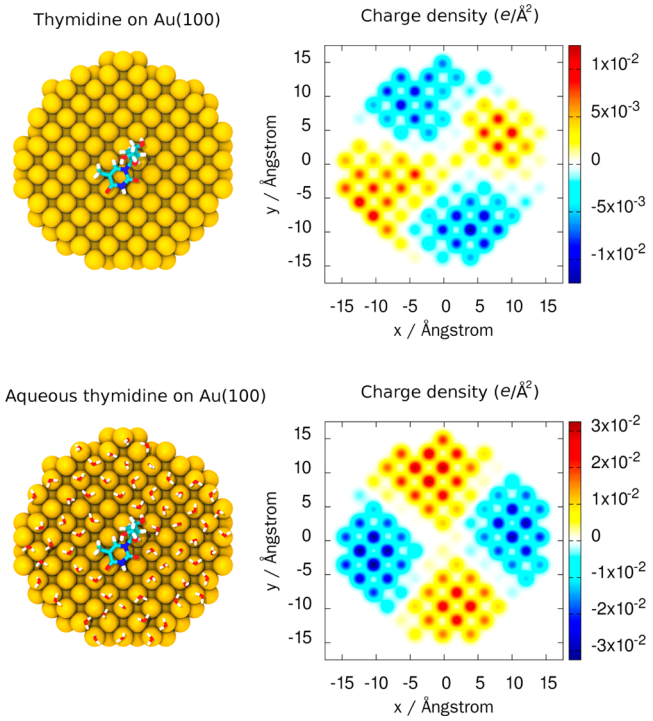

Figure 3. Snapshots and charge distributions of thymidine on a Au(100) surface (top) under vacuum and (bottom) in an aqueous environment. Only the first layer of water is shown for the latter.

dimensional Gaussian functions of point charges located at each Au atom in the first layer. In the absence of water molecules, the thymidine molecule induces positive and negative charge densities on the Au(100) surface, because of its carbonyl, amide, and hydroxyl groups. In the presence of water molecules, the distribution of charge densities is reversed, since the carbonyl and hydroxyl groups of thymidine form hydrogen bonds with surrounding water molecules. However, the separation of positive and negative charges on the Au(100) surface is in the perpendicular direction to the transition dipole moment of the HOMO → LUMO transition which is along the N1−C4−O4 direction (see Figure 2). Differently, the charge distribution on the Au(111) surface is more complicated, because of the fact that the surface Au atoms are more tightly packed and that the two hydroxyl groups of thymidine are both close to the gold surface. Noteworthy, in the absence and the presence of water molecules, the Au(111) surface shows opposite charge separation along the direction to the transition dipole moment of the HOMO → LUMO transition (Figure 4). In the presence of water molecules, the accumulated positive charges at the top-left corner of the Au(111) surface stabilizes

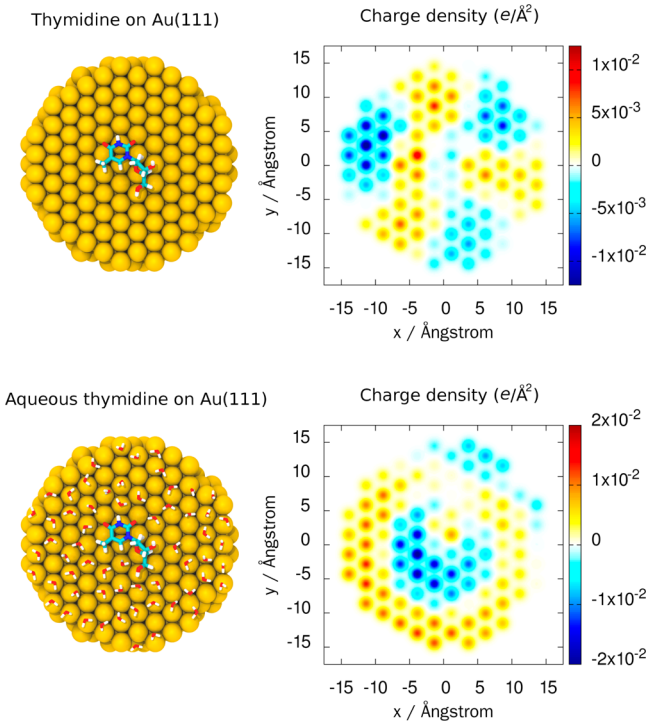

Figure 4. Snapshots and charge distributions of thymidine on a Au(111) surface (top) under vacuum and (bottom) in an aqueous environment. Only the first layer of water is shown for the latter.

the HOMO → LUMO transition and results in a substantial increase in the percentage of the HOMO → LUMO transition in the S_1 state (see Table 5).

4. Comparison of Models for MM Region Interaction. We are further interested in the effects of the damped electrostatic interaction between the QM and metallic MM regions in the DFT/CMM scheme. As listed in Table 6, the use

Table 6. Effects of Damped Potential on the Averaged DFT/MM Interaction Energies for Different Systems[a]

system[b]	$\Delta E_{DFT/MM}$[c] (kcal mol^{-1})	$\Delta E_{exc}(S_1)$ (eV)	$\Delta E_{exc}(S_2)$ (eV)
dT + Au(100)	1.643	0.000	0.000
dT + Au(100) + H_2O	−0.057	0.000	−0.002
dT + Au(111)	0.563	−0.002	0.000
dT + Au(111) + H_2O	0.063	0.001	0.000

[a]The van der Waals interaction is excluded from the DFT/MM interaction energy. [b]"dT" denotes the thymidine molecule. [c]The DFT/MM interaction energy (excluding the van der Waals interaction) is computed by the DFT/CMM approach at the PBE0/def-TZVP level of theory and averaged over 100 snapshots.

of a damped potential leads to diminished interaction energy between QM and MM regions on both Au(100) and Au(111) surfaces under vacuum. The magnitude of the change in the DFT/MM interaction energy is ∼0.6−1.6 kcal mol^{-1}, which is significant, considering the fact that the DFT/MM interaction energy is quite small (between −3.2 kcal mol^{-1} and −3.8 kcal mol^{-1}). In aqueous solutions, however, the effect of the damped potential becomes almost negligible, since the DFT/MM interaction energy gained substantial increase due to the inclusion of the interaction between the nonmetallic MM

dx.doi.org/10.1021/ct400897s | J. Chem. Theory Comput. 2014, 10, 989−1003

region and other parts of the system. We emphasize that the damped potential can put a non-negligible effect (18%−42% decrease) on the interaction potential energy between the QM and metallic MM regions.

The damped potential also puts an effect on charge distributions on gold surfaces. As shown in Figure 5, the use

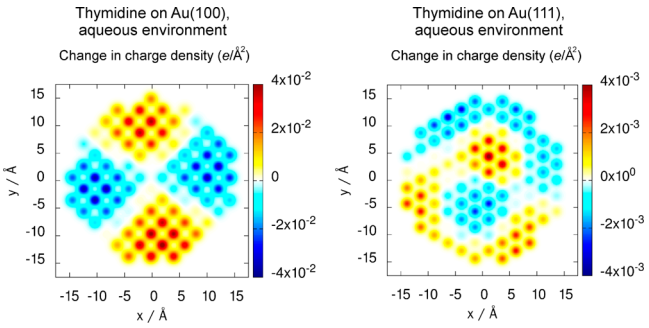

Figure 5. Effects of damped potential on charge distributions of the two gold surfaces in the presence of thymidine and surrounding water molecules.

of a damped potential for thymidine on the Au(100) surface in an aqueous environment results in significantly enhanced charge densities on the surface. However, since the direction of charge separation on the Au(100) surface is perpendicular to the transition dipole moment of the HOMO → LUMO transition of thymidine, the enhanced charge densities show a very subtle effect on the excitation energies of the thymidine molecule (Table 6). The effect of the damped potential on the charge distributions of the Au(111) surface in aqueous environment is 1 order of magnitude smaller (Figure 5), and therefore has also only a subtle effect on the excitation energies of thymidine (Table 6).

■ CONCLUSIONS AND OUTLOOK

Many important physical and chemical phenomena occur at interfaces and constitute the grounds for nanoscience, such as nanophotonics and nanoelectronics, and for nanotechnology in terms of the development of imaging, sensor, and detector devices at the nanoscale. Therefore, the rational design of such interfaces and nanostructures with preassigned properties has become a most essential target for current theory and modeling research. A complicating aspect for such efforts is that these nanostructures often are too small for classical physics to be applicable, while yet being too large to be dealt with by pure quantum chemistry, and they furthermore lack the periodic symmetry that is required for many solid-state physics approaches. Luckily, modern multiscale technology comprising quantum mechanical cores embedded in expedient classical shells that are atomically granulated with force fields and possibly supplemented by dielectric continua, have now been developed to the point where they pose a realistic proposition for applications in nanoscience at interfaces.

The motivation for our work can be found in recent progress of such multiscale methods accommodating also metallic environments. The description of such environments is challenging in that "charge" becomes a meaningless entity and should be replaced with something like an "induced charge". Here, we consider as a fixpoint the recent polarizability−capacitance approach by Jensen and co-workers[17−19] addressing metallic environments and, in particular, their studies using this approach for optical properties of molecules absorbed on silver nanoparticles under vacuum within the time-dependent DFT formalism.[17−19] Their results indicate that the capacitance−polarization model provides an adequate description of static and dynamic response from metallic nanoparticles to external electromagnetic fields, and that computations of metal surface or nanoparticle-induced shifts of molecular properties now are realistic. Our extension of the model addresses molecular systems in complex environments, i.e., consisting from molecules physisorbed on a metal surface or a nanoparticle which, in turn, is placed in a solvent or confined organic/inorganic environment. For the heterogeneous MM region, the capacitance−polarization force field approach is thus employed for the electrostatics and polarization of the metallic part of the MM region with distributed charges in the metallic part and the point charges in the nonmetallic part and where the van der Waals interaction between atoms in the QM and atoms in the MM region as well as between atoms in the MM region is modeled using empirical Lennard-Jones potentials. The outlined model thus includes electrostatic, polarization and van der Waals interactions between the molecules in the QM region, metal surface or nanoparticle in the MM region and solvent molecules in the MM region.

Our approach was illustrated by calculations of optical absorption spectra of thymidine physisorbed on gold surfaces in an aqueous environment. We find a rather significant dependence of the spectral response on the organization of the gold surface and how the metal environment is combined with the aqueous environment. The aqueous environment enhances the difference in the effects of the two gold surfaces. It is clear that the combined effects of the two MM environments are not additive and rather structure- and system-dependent. For example, the overall effects of the Au(111) surface and water molecules lead to a reversal of the S_1 and S_2 states. We find that the induction of charge relocalization of the surface due to the bonding of thymidine covers a quite considerable part of the cluster and that this delocalization is essential for the account of the spectral modification.

We also find that the form, and damping, of the interaction between induced charges and dipoles can be critical for the gold charge distribution and total interaction energies of the system, while, in the present cases, the spectral outcome of damping depends rather subtly on the orientation of the adsorbed molecule and its transition dipole moments.

The present model has rather wide ramifications for modeling of properties and spectra of molecules on surfaces or nanoparticle complexes in solutions or confined environments. The model, as presently implemented, possesses also a few and obvious critical limitations. A precious future development would concern the homogenization of force fields over the entire heterogeneous environment. Thus, in such a future description, the use of conventional nonpolarizable force fields for the nonmetallic part of the MM region should ideally be generalized so that both the metallic and nonmetallic parts of the MM region are included in a uniform fashion using the same capacitance−polarization model. Such a description would allow to account for charge transfer between the metallic and nonmetallic parts of the MM region and open the model for systems with strong chemisorption.

APPENDIX A: ELECTROSTATIC INTERACTION TENSORS IN CAPACITANCE−POLARIZATION MODEL

The DFT/CMM approach describes heterogeneous metallic and non-metallic MM region using a capacitance−polarization model for its metallic part and a conventional force field for its non-metallic part. In the capacitance−polarization model,[16,31] distributed charges and distributed dipoles are described by Gaussian distributions:

$$q_m(\mathbf{r}) = \frac{q_m}{\pi^3 R_q^3}\exp\left(-\frac{|\mathbf{r}-\mathbf{r}_m|^2}{R_q^2}\right)$$

$$\mathbf{p}_m(\mathbf{r}) = \frac{1}{\pi^{3/2}R_p^3}\mathbf{p}_m\cdot\nabla\exp\left(-\frac{|\mathbf{r}-\mathbf{r}_m|^2}{R_p^2}\right) \quad \text{(A-1)}$$

where R_q and R_p are the charge and the dipole distribution widths, respectively. Interaction tensors, which enter the expression for the metallic MM region energy definition and the Relay matrix expression for distributed charges and polarizabilities, have been derived by Mayer;[31] here, we present only the final expressions for these tensors omitting the detailed derivation. Following the work of Mayer,[31] the electrostatic interaction between distributed charges in the metallic part of the MM region is given by the following expression:

$$T_{mn}^{qq} = \frac{\mathrm{erf}(|\mathbf{r}_m-\mathbf{r}_n|/R_{qq})}{|\mathbf{r}_m-\mathbf{r}_n|} \quad \text{(A-2)}$$

The interaction between distributed charge and distributed dipole in the metallic part of the MM region is given by the expression

$$T_{mn}^{qp} = -\frac{\mathbf{r}_m-\mathbf{r}_n}{|\mathbf{r}_m-\mathbf{r}_n|^3}\left[\mathrm{erf}\left(\frac{|\mathbf{r}_m-\mathbf{r}_n|}{R_{qp}}\right) - \frac{2|\mathbf{r}_m-\mathbf{r}_n|}{\sqrt{\pi}R_{qp}}\exp\left(-\frac{|\mathbf{r}_m-\mathbf{r}_n|^2}{R_{qp}^2}\right)\right] \quad \text{(A-3)}$$

and the interaction between two distributed dipoles in the metallic part of the MM region is given by the expression

$$\mathbf{T}_{mn}^{pp} = \frac{3(\mathbf{r}_m-\mathbf{r}_n)\otimes(\mathbf{r}_m-\mathbf{r}_n) - |\mathbf{r}_m-\mathbf{r}_n|^2\mathbf{I}}{|\mathbf{r}_m-\mathbf{r}_n|^5}\left[\mathrm{erf}\left(\frac{|\mathbf{r}_m-\mathbf{r}_n|}{R_{pp}}\right) - \frac{2|\mathbf{r}_m-\mathbf{r}_n|}{\sqrt{\pi}R_{pp}}\exp\left(-\frac{|\mathbf{r}_m-\mathbf{r}_n|^2}{R_{qp}^2}\right)\right] - \frac{4}{\sqrt{\pi}R_{pp}^3}\frac{(\mathbf{r}_m-\mathbf{r}_n)\otimes(\mathbf{r}_m-\mathbf{r}_n)}{|\mathbf{r}_m-\mathbf{r}_n|^2}\exp\left(-\frac{|\mathbf{r}_m-\mathbf{r}_n|^2}{R_{qp}^2}\right) \quad \text{(A-4)}$$

In the above equations, we introduced effective Gaussian distribution widths $R_{qq} = \sqrt{2}R_q$, $R_{qp} = (R_q^2 + R_p^2)^{1/2}$ and $R_p = \sqrt{2}R_p$ for charge−charge, charge-dipole and dipole−dipole interactions, respectively. After describing the interaction tensors between distributed charges and dipoles in the metallic part of the MM region, we turn to the remaining two cases, namely, the tensors used to describe the interaction between distributed charges/dipoles in the metallic part of the MM region and point charges in the non-metallic part of the MM region, and conventional interaction tensors used to describe the interaction between point charges in the non-metallic part of the MM region. According to Mayer the interaction between distributed and point charges can be written as

$$T_{mn}^{q} = \frac{\mathrm{erf}(|\mathbf{r}_m-\mathbf{r}_n|/R_q)}{|\mathbf{r}_m-\mathbf{r}_n|} \quad \text{(A-5)}$$

and the interaction between the distributed dipole and point charge can be written as

$$\mathbf{T}_{mn}^{p} = \frac{(\mathbf{r}_m-\mathbf{r}_n)}{|\mathbf{r}_m-\mathbf{r}_n|^3}\left[\mathrm{erf}\left(\frac{|\mathbf{r}_m-\mathbf{r}_n|}{R_p}\right) - \frac{2|\mathbf{r}_m-\mathbf{r}_n|}{\sqrt{\pi}R_p}\exp\left(-\frac{|\mathbf{r}_m-\mathbf{r}_n|^2}{R_p^2}\right)\right] \quad \text{(A-6)}$$

Finally, for the sake of completeness, we also give the conventional interaction tensor between point charges in the non-metallic part of the MM region, which reads as

$$T_{mn} = \frac{1}{|\mathbf{r}_m-\mathbf{r}_n|} \quad \text{(A-7)}$$

After describing interaction tensors between various quantities (distributed charges, distributed dipoles, and point charges) in the MM region, let us turn our attention to the description of interaction between electrons in the QM region and permanent and induced charges and also the induced dipoles in the MM region. The interaction operator between permanent charges and electrons in the DFT/CMM approach has the same form as in the conventional QM/MM methods, and can be written as

$$\hat{T}_m(\mathbf{r}) = \frac{1}{|\mathbf{r}_m-\mathbf{r}_n|} \quad \text{(A-8)}$$

The integrals over the $\hat{T}_m(\mathbf{r})$ operation can be easily computed following the same procedure as that used for evaluation of the nuclear potential integrals in the Kohn−Sham method. The remaining two operators, which enter the general expression for the QM/MM contribution to the Kohn−Sham operator, are dependent on induced charges and induced dipoles, which are described by Gaussian distribution functions, and thus have the following more-complex forms:

$$\hat{T}_m^q(\mathbf{r}) = \frac{\mathrm{erf}(|\mathbf{r}-\mathbf{r}_m|/R_q)}{|\mathbf{r}-\mathbf{r}_m|}$$

and

$$\hat{\mathbf{T}}_m^p = \frac{\mathbf{r}-\mathbf{r}_m}{|\mathbf{r}-\mathbf{r}_m|}\left[\mathrm{erf}\left(\frac{|\mathbf{r}-\mathbf{r}_m|}{R_p}\right) - \frac{2|\mathbf{r}-\mathbf{r}_m|}{\sqrt{\pi}R_p}\exp\left(-\frac{|\mathbf{r}-\mathbf{r}_m|^2}{R_p^2}\right)\right] \quad \text{(A-9)}$$

respectively. Unfortunately, evaluation of integrals over the last two operators is not possible in conventional quantum chemistry programs, and we have been forced to derive and implement an appropriate scheme for computation of the integrals over these operators. The final results of this derivation are presented in Appendix B.

APPENDIX B: FORMULAE FOR EVALUATION OF DAMPED ELECTROSTATIC INTERACTION BETWEEN QM AND METALLIC MM REGIONS

The induced charges and dipoles in the capacitance−polarization model are described by Gaussian distributions with

dx.doi.org/10.1021/ct400897s | J. Chem. Theory Comput. 2014, 10, 989−1003

specific widths, and their interaction with electrons in the QM region are described by the operators $\hat{T}_m^q$ and $\hat{\mathbf{T}}_m^p$. Here, we describe a computational procedure for evaluation of the one-electron integrals over these operators. First, we write the total potential generated by induced charges and dipoles in the following form:

$$V(r) = \sum_m q_m^{\mathrm{ind}} \frac{\mathrm{erf}(|\mathbf{r} - \mathbf{r}_m|/R_q)}{|\mathbf{r} - \mathbf{r}_m|} + \sum_m q_m^{\mathrm{ind}} \frac{(\mathbf{r} - \mathbf{r}_m)}{|\mathbf{r} - \mathbf{r}_m|^2} \times \left[\frac{\mathrm{erf}(|\mathbf{r} - \mathbf{r}_m|/R_p)}{|\mathbf{r} - \mathbf{r}_m|} - \frac{2}{\sqrt{\pi} R_p} \exp\left(-|\mathbf{r} - \mathbf{r}_m|^2/R_p^2\right) \right] \quad \text{(B-1)}$$

Integration of above-given potential over Gaussian-type orbitals can be carried out following a similar procedure as that used for evaluation of nuclear potential integrals. Thus, in the first step in the evaluation of these integrals, the operator $\hat{T}_m^q$ is transformed using a Laplace transformation

$$U^0(\mathbf{r}, \mathbf{M}, R_q) = \frac{\mathrm{erf}(|\mathbf{r} - \mathbf{M}|/R_q)}{|\mathbf{r} - \mathbf{M}|} = \frac{2}{\sqrt{\pi}} \int_0^{1/R_q} \exp(-s^2 |\mathbf{r} - \mathbf{M}|^2) \mathrm{d}s \quad \text{(B-2)}$$

where the transformed form of the operator $\hat{\mathbf{T}}_m^p$ is obtained using the following relationship:

$$\mathbf{U}^{(1)}(\mathbf{r}, \mathbf{M}, R_p) = \nabla_{\mathrm{M}} U^{(0)}(\mathbf{r}, \mathbf{M}, R_p) \quad \text{(B-3)}$$

Here, we introduced the new notation $\mathbf{M}$ for the position vector of the mth atom in the metallic part of the MM region. Taking into account the above-given form of the Laplace-transformed operators $\hat{T}_m^q$ and $\hat{\mathbf{T}}_l$, the combined integral of these operators over two Gaussian functions centered on atoms A and B in the QM region can be written as

$$(a|V_m|b) = q_m^{\mathrm{ind}} \int \phi_a(\mathbf{r}, \mathbf{A}) \phi_b(\mathbf{r}, \mathbf{B}) U^0(\mathbf{r}, \mathbf{M}, R_q) \mathrm{d}\mathbf{r} + \sum_{\lambda=x,y,z} p_{m,\lambda}^{\mathrm{ind}} \int \phi_a(\mathbf{r}, \mathbf{A}) \phi_b(\mathbf{r}, \mathbf{B}) U_\lambda^1(\mathbf{r}, \mathbf{M}, R_p) \mathrm{d}\mathbf{r} \quad \text{(B-4)}$$

where we introduced the Gaussian orbitals $\phi_a(\mathbf{r},\mathbf{A})$ and $\phi_b(\mathbf{r},\mathbf{B})$ centered on atoms A and B in the QM region, respectively. The above given integral can be easily computed using the McMurchie−Davidson scheme,[35] in which the Gaussian orbitals expanded in Hermite Gaussians and a one-center recurrent relation is applied to the auxiliary integrals of the following type:

$$[\overline{0}]^{(m)} = \frac{\sqrt{2}\pi}{\eta^{3/2}} \left(\frac{2\eta}{1 + \eta R_q^2} \right)^{m+1/2} F_m\left(\frac{\eta}{1 + \eta R_q^2} |\mathbf{P} - \mathbf{M}^2| \right), \quad \text{(B-5)}$$

where $\eta = \alpha + \beta$ is the sum of the primitive exponents, $\mathbf{P} = (\alpha\mathbf{A} + \beta\mathbf{B})/\eta$ is the center of the Hermite expansion and F_m is the usual Boys' function.

AUTHOR INFORMATION

Corresponding Author

*Tel.: +46 (0)8 5537 8418. Fax: +46 (0)8 5537 8590. E-mail: rinkevic@theochem.kth.se.

Notes

The authors declare no competing financial interest.

REFERENCES

(1) Barone, V.; Improta, R.; Rega, N. *Acc. Chem. Res.* **2008**, *41*, 605.
(2) Nielsen, C. B.; Christiansen, O.; Mikkelsen, K. V.; Kongsted, J. *J. Chem. Phys.* **2007**, *126*, 154112.
(3) Lipparini, F.; Cappelli, C.; Barone, V. *J. Chem. Theory Comput.* **2012**, *8*, 4153.
(4) Steindal, A. H.; Ruud, K.; Frediani, L.; Aidas, K.; Kongsted, J. *J. Phys. Chem. B* **2011**, *115*, 3027.
(5) Gagliardi, L.; Lindh, R.; Karlstrom, G. *J. Chem. Phys.* **2004**, *121*, 4494.
(6) Gao, J.; Amara, P.; Alhambra, C.; Field, M. J. *J. Phys. Chem. A* **1998**, *102*, 4714.
(7) Kairys, V.; Jensen, J. H. *J. Phys. Chem. A* **2000**, *104*, 6656.
(8) Laio, A.; VandeVondele, J.; Rothlisberger, U. *J. Chem. Phys.* **2002**, *116*, 6941.
(9) Reuter, N.; Dejaegere, A.; Maigret, B.; Karplus, M. *J. Phys. Chem. A* **2000**, *104*, 1720.
(10) Senn, H. M.; Thiel, W. *Angew. Chem., Int. Ed.* **2009**, *48*, 1198.
(11) Murugan, N. A.; Apostolov, R.; Rinkevicius, Z.; Kongsted, J.; Lindahl, E.; Ågren, H. *J. Am. Chem. Soc.* **2013**, *135*, 13590.
(12) Rinkevicius, Z.; Frecuş, B.; Murugan, N. A.; Vahtras, O.; Kongsted, J.; Ågren, H. *J. Chem. Theory Comput.* **2011**, *8*, 257.
(13) Steindal, A. H.; Olsen, J. M. H.; Ruud, K.; Frediani, L.; Kongsted, J. *Phys. Chem. Chem. Phys.* **2012**, *14*, 5440.
(14) Kresse, G.; Furthmüller, J. *Phys. Rev. B* **1996**, *54*, 11169.
(15) José, M. S.; Emilio, A.; Julian, D. G.; Alberto, G.; Javier, J.; Pablo, O.; Daniel, S.-P. *J. Phys.: Condens. Matter* **2002**, *14*, 2745.
(16) Jensen, L. L.; Jensen, L. *J. Phys. Chem. C* **2008**, *112*, 15697.
(17) Morton, S. M.; Jensen, L. *J. Chem. Phys.* **2010**, *133*, 074103.
(18) Morton, S. M.; Jensen, L. *J. Chem. Phys.* **2011**, *135*, 134103.
(19) Payton, J. L.; Morton, S. M.; Moore, J. E.; Jensen, L. *J. Chem. Phys.* **2012**, *136*, 214103.
(20) Mie, G. *Ann. Phys.* **1908**, *330*, 377.
(21) Bian, R. X.; Dunn, R. C.; Xie, X. S.; Leung, P. T. *Phys. Rev. Lett.* **1995**, *75*, 4772.
(22) Yang, W.-H.; Schatz, G. C.; Van Duyne, R. P. *J. Chem. Phys.* **1995**, *103*, 869.
(23) Morton, S. M.; Silverstein, D. W.; Jensen, L. *Chem. Rev.* **2011**, *111*, 3962.
(24) Corni, S.; Tomasi, J. *J. Chem. Phys.* **2001**, *114*, 3739.
(25) Jorgensen, S.; Ratner, M. A.; Mikkelsen, K. V. *J. Chem. Phys.* **2001**, *115*, 3792.
(26) Neuhauser, D.; Lopata, K. *J. Chem. Phys.* **2007**, *127*, 154715.
(27) Masiello, D. J.; Schatz, G. C. *Phys. Rev. A* **2008**, *78*, 042505.
(28) Arcisauskaite, V.; Kongsted, J.; Hansen, T.; Mikkelsen, K. V. *Chem. Phys. Lett.* **2009**, *470*, 285.
(29) Golze, D.; Iannuzzi, M.; Nguyen, M.-T.; Passerone, D.; Hutter, J. *J. Chem. Theory Comput.* **2013**, *9* (11), 5086−5097.
(30) Jensen, L.; Åstrand, P.-O.; Mikkelsen, K. V. *Int. J. Quantum Chem.* **2001**, *84*, 513.
(31) Mayer, A. *Phys. Rev. B* **2007**, *75*, 045407.
(32) Kongsted, J.; Osted, A.; Mikkelsen, K. V.; Christiansen, O. V. E. *Mol. Phys.* **2002**, *100*, 1813.
(33) Lin, H.; Truhlar, D. *Theor. Chem. Acc.* **2007**, *117*, 185.
(34) Ahlström, P.; Wallqvist, A.; Engström, S.; Jönsson, B. *Mol. Phys.* **1989**, *68*, 563.
(35) McMurchie, L. E.; Davidson, E. R. *J. Comput. Phys.* **1978**, *26*, 218.
(36) Jansik, B.; Jonsson, D.; Salek, P.; Agren, H. *J. Chem. Phys.* **2004**, *121*, 7595.
(37) Rinkevicius, Z.; Tunell, I.; Salek, P.; Vahtras, O.; Agren, H. *J. Chem. Phys.* **2003**, *119*, 34.
(38) Salek, P.; Vahtras, O.; Helgaker, T.; Agren, H. *J. Chem. Phys.* **2002**, *117*, 9630.
(39) Tunell, I.; Rinkevicius, Z.; Vahtras, O.; Salek, P.; Helgaker, T.; Agren, H. *J. Chem. Phys.* **2003**, *119*, 11024.

(40) Plekan, O.; Feyer, V.; Ptasińska, S.; Tsud, N.; Cháb, V. R.; Matolín, V. R.; Prince, K. C. *J. Phys. Chem. C* **2010**, *14*, 15036.
(41) Bogdan, D.; Morari, C. *J. Phys. Chem. C* **2012**, *116*, 7351.
(42) Avvakumova, S.; Scari, G.; Porta, F. *RSC Adv.* **2012**, *2*, 3658.
(43) MacKerell, A. D.; Bashford, D.; Bellott; Dunbrack, R. L.; Evanseck, J. D.; Field, M. J.; Fischer, S.; Gao, J.; Guo, H.; Ha, S.; Joseph-McCarthy, D.; Kuchnir, L.; Kuczera, K.; Lau, F. T. K.; Mattos, C.; Michnick, S.; Ngo, T.; Nguyen, D. T.; Prodhom, B.; Reiher, W. E.; Roux, B.; Schlenkrich, M.; Smith, J. C.; Stote, R.; Straub, J.; Watanabe, M.; Wiórkiewicz-Kuczera, J.; Yin, D.; Karplus, M. *J. Phys. Chem. B* **1998**, *102*, 3586.
(44) Mackerell, A. D.; Feig, M.; Brooks, C. L. *J. Comput. Chem.* **2004**, *25*, 1400.
(45) Wright, L. B.; Rodger, P. M.; Corni, S.; Walsh, T. R. *J. Chem. Theory Comput.* **2013**, *9*, 1616.
(46) Hess, B.; Kutzner, C.; van der Spoel, D.; Lindahl, E. *J. Chem. Theory Comput.* **2008**, *4*, 435.
(47) Bussi, G.; Donadio, D.; Parrinello, M. *J. Chem. Phys.* **2007**, *126*, 014101.
(48) Darden, T.; York, D.; Pedersen, L. *J. Chem. Phys.* **1993**, *98*, 10089.
(49) Essmann, U.; Perera, L.; Berkowitz, M. L.; Darden, T.; Lee, H.; Pedersen, L. G. *J. Chem. Phys.* **1995**, *103*, 8577.
(50) Jorgensen, W. L.; Chandrasekhar, J.; Madura, J. D.; Impey, R. W.; Klein, M. L. *J. Chem. Phys.* **1983**, *79*, 926.
(51) Aidas, K.; Angeli, C.; Bak, K. L.; Bakken, V.; Bast, R.; Boman, L.; Christiansen, O.; Cimiraglia, R.; Coriani, S.; Dahle, P.; Dalskov, E. K.; Ekström, U.; Enevoldsen, T.; Eriksen, J. J.; Ettenhuber, P.; Fernández, B.; Ferrighi, L.; Fliegl, H.; Frediani, L.; Hald, K.; Halkier, A.; Hättig, C.; Heiberg, H.; Helgaker, T.; Hennum, A. C.; Hettema, H.; Hjertenæs, E.; Høst, S.; Høyvik, I.-M.; Iozzi, M. F.; Jansík, B.; Jensen, H. J. A.; Jonsson, D.; Jørgensen, P.; Kauczor, J.; Kirpekar, S.; Kjærgaard, T.; Klopper, W.; Knecht, S.; Kobayashi, R.; Koch, H.; Kongsted, J.; Krapp, A.; Kristensen, K.; Ligabue, A.; Lutnæs, O. B.; Melo, J. I.; Mikkelsen, K. V.; Myhre, R. H.; Neiss, C.; Nielsen, C. B.; Norman, P.; Olsen, J.; Olsen, J. M. H.; Osted, A.; Packer, M. J.; Pawlowski, F.; Pedersen, T. B.; Provasi, P. F.; Reine, S.; Rinkevicius, Z.; Ruden, T. A.; Ruud, K.; Rybkin, V. V.; Sałek, P.; Samson, C. C. M.; de Merás, A. S.; Saue, T.; Sauer, S. P. A.; Schimmelpfennig, B.; Sneskov, K.; Steindal, A. H.; Sylvester-Hvid, K. O.; Taylor, P. R.; Teale, A. M.; Tellgren, E. I.; Tew, D. P.; Thorvaldsen, A. J.; Thøgersen, L.; Vahtras, O.; Watson, M. A.; Wilson, D. J. D.; Ziolkowski, M.; Ågren, H. *Wiley Interdiscip. Rev.: Comput. Mol. Sci.* **2013**, DOI: 10.1002/wcms.1172.
(52) Adamo, C.; Barone, V. *J. Chem. Phys.* **1999**, *110*, 6158.
(53) Schafer, A.; Huber, C.; Ahlrichs, R. *J. Chem. Phys.* **1994**, *100*, 5829.
(54) Gustavsson, T.; Bányász, Á.; Lazzarotto, E.; Markovitsi, D.; Scalmani, G.; Frisch, M. J.; Barone, V.; Improta, R. *J. Am. Chem. Soc.* **2005**, *128*, 607.